

## SHORT-LIVED STAR-FORMING GIANT CLUMPS IN COSMOLOGICAL SIMULATIONS OF $z \approx 2$ DISKS

SHY GENEL<sup>1</sup>, THORSTEN NAAB<sup>2</sup>, REINHARD GENZEL<sup>1,3</sup>, NATASCHA M. FÖRSTER SCHREIBER<sup>1</sup>, AMIEL STERNBERG<sup>4</sup>, LUDWIG OSER<sup>2,5</sup>, PETER H. JOHANSSON<sup>5</sup>, ROMEEL DAVÉ<sup>6</sup>, BENJAMIN D. OPPENHEIMER<sup>7</sup>, ANDREAS BURKERT<sup>5</sup>

*The Astrophysical Journal Letters, submitted*

### ABSTRACT

Many observed massive star-forming  $z \approx 2$  galaxies are large disks that exhibit irregular morphologies, with  $\approx 1$  kpc,  $\approx 10^{8-10} M_{\odot}$  clumps. We present high-resolution cosmological SPH simulations that zoom-in on the formation of individual  $M_{*} \approx 10^{10.5} M_{\odot}$  galaxies in  $\approx 10^{12} M_{\odot}$  halos at  $z \approx 2$ . Our code includes strong stellar feedback parameterized as momentum-driven galactic winds. This model reproduces many characteristic features of this observed class of galaxies, such as their clumpy morphologies, high gas fractions ( $f_g \approx 30\%$ ) and high specific star-formation rates ( $\approx 1 \text{ Gyr}^{-1}$ ). In accord with recent models, giant clumps ( $M_{\text{clump}} \gtrsim 5 \times 10^8 M_{\odot}$ ) form in-situ via gravitational instability. However, the galactic winds are critical for their subsequent evolution. In the cases we have studied, the clumps are short-lived and are disrupted by wind-driven mass loss. They do not virialise or migrate to the galaxy centers as suggested in recent work neglecting strong winds. Our simulations agree well with new observational constraints on clump kinematics and with the detection of winds from high-redshift galaxies and in particular from individual clumps.

*Subject headings:* galaxies: evolution — galaxies: formation — galaxies: high-redshift — galaxies: structure

### 1. INTRODUCTION

Star-forming disk galaxies at  $z \approx 2$  differ from their local counterparts in several aspects: they are more gas-rich and rapidly star-forming, and have irregular morphologies and high gas velocity dispersions. Spatially resolved observations of their rest-frame UV and optical continuum light often reveal large ( $\approx 1$  kpc) clumps (Elmegreen et al. 2005). Clumpy morphologies are also observed with star-formation tracers such as H $\alpha$  (e.g. the SINS survey; Förster Schreiber et al. 2009). The spectrally resolved line emissions reveal ordered rotation and high velocity dispersions, arguably tracing gas-phase turbulence (Genzel et al. 2006, 2008; Förster Schreiber et al. 2006; Shapiro et al. 2008; Cresci et al. 2009).

Theoretically, the large  $z \approx 2$  star-forming galaxies have been considered as marginally-unstable thick disks, where the large random motions set the large masses and sizes for unstable regions collapsing into giant clumps (Bournaud et al. 2007, 2008; Genzel et al. 2008; Elmegreen et al. 2008; Burkert et al. 2010; Agertz et al. 2009; Dekel et al. 2009b; Ceverino et al. 2010). In this picture, the high star-formation rates result from the high growth rates of cosmic structures at  $z \approx 2$  (Genel et al. 2008), as gas funnels directly from the cosmic web to the vicinity of galaxies in a 'cold-mode' accretion (Kereš et al. 2005; Dekel et al. 2009a). However, several observational hints have not yet been addressed in this

framework. First, vigorous outflows are observed from a variety of star-forming galaxies at high redshift, both globally (e.g. Pettini et al. 2000; Steidel et al. 2010) and also from individual giant clumps (Genzel et al. in prep.). Second, high signal-to-noise observations of individual giant clumps reveal only minor kinematical signatures, sometimes indicating dynamical masses lower than alternative independent clump mass estimates (Genzel et al. in prep.). Third, abundance matching of galaxies and dark matter halos suggests that at  $z \approx 2$ , much like at  $z = 0$ , typically not more than  $\approx 20\%$  of the baryons associated with halos of any mass have turned into stars (Moster et al. 2010), causing some tension with the high efficiency of 'cold-mode' accretion.

A crucial issue is whether giant clumps survive long enough to become stellar-dominated and/or sink to their galaxies' centers, contributing to the buildup of bulges (Immeli et al. 2004; Genzel et al. 2008; Dekel et al. 2009b; Shapiro et al. 2010; Murray et al. 2010; Krumholz & Dekel 2010). Conflicting theoretical claims have been made, while observations are not yet conclusive. However, none of the cosmological or isolated simulations reported so far (but see Sales et al. 2010), which find long-lived migrating clumps, included strong feedback from star-formation. As the 'clumpy phase' appears to be ubiquitous at  $z \approx 1-3$ , it is of fundamental importance for our understanding of galaxy formation to know what role giant clumps play in building bulges/spheroids.

In this Letter, we demonstrate as a proof of principle, that incorporating galactic superwinds resulting from stellar feedback into the existing theoretical picture, can have important implications for our understanding of  $z \approx 2$  disks and their evolution. We use hydrodynamical cosmological simulations to investigate the formation and properties of a small sample of star-forming disks. Comparing to observed galaxies, we conclude that the giant clumps may be short-lived transient features, due to the strong feedback (which is observed at high redshift). In an upcoming paper, we will present a comprehensive study of parameter space and resolution, study the relationship between halo formation histories and the characteristics of their central galaxies, and perform a broader com-

<sup>1</sup> Max Planck Institut für extraterrestrische Physik, Giessenbachstrasse, 85748 Garching, Germany; shy@mpe.mpg.de; genzel@mpe.mpg.de; forster@mpe.mpg.de

<sup>2</sup> Max Planck Institut für Astrophysik, Karl-Schwarzschild-Str. 1, 85741 Garching, Germany; naab@mpa-garching.mpg.de; oser@usm.lmu.de

<sup>3</sup> Department of Physics, Le Conte Hall, University of California, Berkeley, CA 94720

<sup>4</sup> School of Physics and Astronomy, Tel Aviv University, Tel Aviv 69978, Israel; amiel@wise.tau.ac.il

<sup>5</sup> Universitäts-Sternwarte München, Scheinerstr. 1, D-81679 München, Germany; pjohan@usm.lmu.de; burkert@usm.lmu.de

<sup>6</sup> Astronomy department, University of Arizona, Tuscon, AZ 85721; rad@as.arizona.edu

<sup>7</sup> Leiden Observatory, Leiden University, PO Box 9513, 2300 RA Leiden, the Netherlands; oppenheimer@strw.leidenuniv.nl

parison with observations.

## 2. THE SIMULATIONS: CODE AND SETUP

We run ‘zoom-in’ cosmological simulations focused on individual halos taken from the  $72h^{-1}$  Mpc cosmological dark matter simulation presented in Oser et al. (2010) that uses the following cosmological parameters:  $\Omega_m = 0.26$ ,  $\Omega_\Lambda = 0.74$ ,  $\Omega_b = 0.044$ ,  $h = 0.72$ ,  $n = 0.95$  and  $\sigma_8 = 0.77$ . As we focus on massive disks with high star-formation rates (SFR), we select  $\approx 10^{12} M_\odot$  halos at  $z = 2$  with no major merger (mass ratio  $> 1:3$ ) since  $z = 3$  and instantaneous dark matter growth rates exceeding  $500 M_\odot \text{ yr}^{-1}$  (see Genel et al. 2008). These criteria are met by  $\approx 15\%$  of the halos in the relevant mass bin, i.e. our galaxies form in halos that are neither the most ‘typical’ nor very ‘special’ or rare. From this sample, we randomly selected six halos and generated ‘zoom-in’ initial conditions (as in Oser et al. 2010) for re-simulations including baryons, with mass resolution of  $8 \times 10^5 M_\odot$  and  $5 \times 10^6 M_\odot$  for baryonic and high-resolution dark matter particles, respectively. The gravitational softening lengths of baryonic particles are  $200h^{-1}$  pc, constant in comoving units, resulting in physical softening lengths of  $\approx 90$  pc at  $z = 2$ .

The cosmological box is evolved to  $z = 2$  with the extended N-body/SPH code *Gadget-2* (Springel 2005) version of Oppenheimer & Davé (2006, 2008). This version includes ionisation and heating by a uniform background radiation (Haardt & Madau 2001) in the optically thin limit, atomic cooling down to  $T = 10^4 K$  from hydrogen and metals, star-formation and feedback, as well as mass loss and metal enrichment from AGB stars and supernovae of types II and Ia.

The Springel & Hernquist (2003) star-formation model used in Oppenheimer & Davé (2008), which has a stiff effective equation of state, is replaced by the Schaye & Dalla Vecchia (2008) approach. There, the usual cooling and heating operate at  $\rho < \rho_{EOS}$ , while for  $\rho > \rho_{EOS}$  a polytropic equation of state with  $\gamma = 4/3$  is implemented. This ensures that the (thermal) Jeans mass  $M_J$  remains constant with varying density and does not become unresolved. Here  $\rho_{EOS} = 0.1 \text{ cm}^{-3}$  is defined such that  $M_J \approx 1.4 \times 10^7 M_\odot$  at  $\rho = \rho_{EOS}$  and  $T = 10^4 K$ . Star-formation is parameterised as

$$\frac{d\rho_*}{dt} = \frac{\rho}{1 \text{ Gyr}} \left(\frac{\rho}{\rho_{th}}\right)^{1.26}, \quad (1)$$

with the star-formation density threshold  $\rho_{th} = \rho_{EOS} = 0.1 \text{ cm}^{-3}$ , which reproduces the Kennicutt (1998) 2D star-formation relation (Schaye & Dalla Vecchia 2008). In addition, we calculate the local minimum (of all directions) gas surface density  $\rho^2/|\nabla\rho|$  (Gnedin et al. 2009), and suppress star-formation if  $\rho^2/|\nabla\rho| < 10^{21} \text{ cm}^{-2}$ .

The feedback scheme developed by Oppenheimer & Davé (2006, 2008) builds on the kinetic feedback scheme of Springel & Hernquist (2003), where star-forming gas particles are stochastically kicked with velocities in the  $\mathbf{v} \times \mathbf{a}$  direction, where  $\mathbf{v}$  is the particle’s velocity prior to the kick and  $\mathbf{a}$  its acceleration. Subsequently, they are decoupled from hydrodynamics for a short time to allow them to propagate out of their star-formation sites and eventually leave their galaxies. Oppenheimer & Davé (2006) used this mechanism with a significant change to the two parameters that control the wind. In their model, the magnitude of the kick is  $v_{wind} = \sigma(2 + 3\sqrt{f_L - 1})$  and the mass-loading factor

$$\frac{\dot{M}_W}{SFR} \equiv \eta = \frac{\sigma_0}{\sigma}, \quad (2)$$

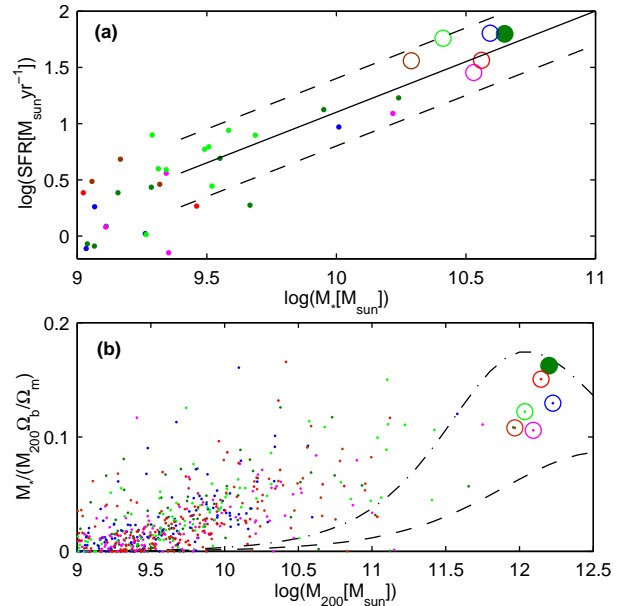


FIG. 1.— Global properties of six ‘zoom-in’ simulations at  $z = 2$ . *Top*: SFR versus stellar mass. Each color represents one simulation, with its central galaxy (circles) and the smaller galaxies in its vicinity (dots). The observed Daddi et al. (2007) relation (solid; standard deviation is dashed) is re-normalised by 0.3 dex downwards (see text). *Bottom*: ‘Baryon conversion efficiency’ as a function of halo mass. The highest efficiency of  $\approx 15\%$  is obtained at  $M_{halo} \gtrsim 10^{12} M_\odot$ , in rough agreement with observations (Moster et al. 2010;  $z = 2.5$  in dashed black and  $z = 0$  in dashed-dotted black). The most massive high-resolution halo in each simulation is marked with a circle. The colors are as in the top panel. In both panels s224 is marked with a filled circle.

where  $f_L \approx 1 - 2$  is the luminosity factor,  $\sigma$  is the ‘velocity dispersion’ of the galaxy that is calculated from its mass based on an on-the-fly group finder<sup>8</sup>, and  $\sigma_0$  is a constant (here  $\sigma_0 = 300 \text{ km s}^{-1}$ ). Introducing  $\sigma$ -dependencies, these two parameters scale with the mass of the galaxy, following the theory of momentum-driven winds induced by the radiation pressure from young stars (Murray et al. 2005; Zhang & Thompson 2010), and in accordance with observational evidence (e.g. Martin 2005; Rupke et al. 2005). The Oppenheimer & Davé (2006) model reproduces the observed metal enrichment of the intergalactic medium at  $2 < z < 5$  and the galaxy mass-metallicity relation (Finlator & Davé 2008).

We use  $v_{wind} = \sigma(4 + 4.29\sqrt{f_L - 1})$ , which ensures that wind particles can escape their galaxy, and gives typical velocities of  $\approx 350 - 750 \text{ km s}^{-1}$  for the central galaxies considered. We also ensure that the velocity kicks are perpendicular to the disk by calculating  $\mathbf{v} \times \mathbf{a}$  in the inertial frame of the galaxy.

## 3. RESULTS

In this section we focus on a central galaxy of one of our halos, named s224, that is typical of our sample. We will discuss our full sample in detail elsewhere, but we briefly describe some global properties here. In Figure 1, panel (a) shows the SFR- $M_*$  plane for galaxies in the high-resolution region. Stellar masses and SFRs are measured by the on-the-fly group finder. The simulated galaxies populate the same region as observed  $z \approx 2$  galaxies, according to the Daddi et al. (2007) relation (solid) re-normalised by 0.3 dex downwards

<sup>8</sup> For calculation efficiency, a Friends-of-friends (FOF) algorithm is used, with a linking length  $b = 0.025(\frac{H(z)}{H(0)})^{1/3}$  that is calibrated to the SKID group finder at various redshifts.

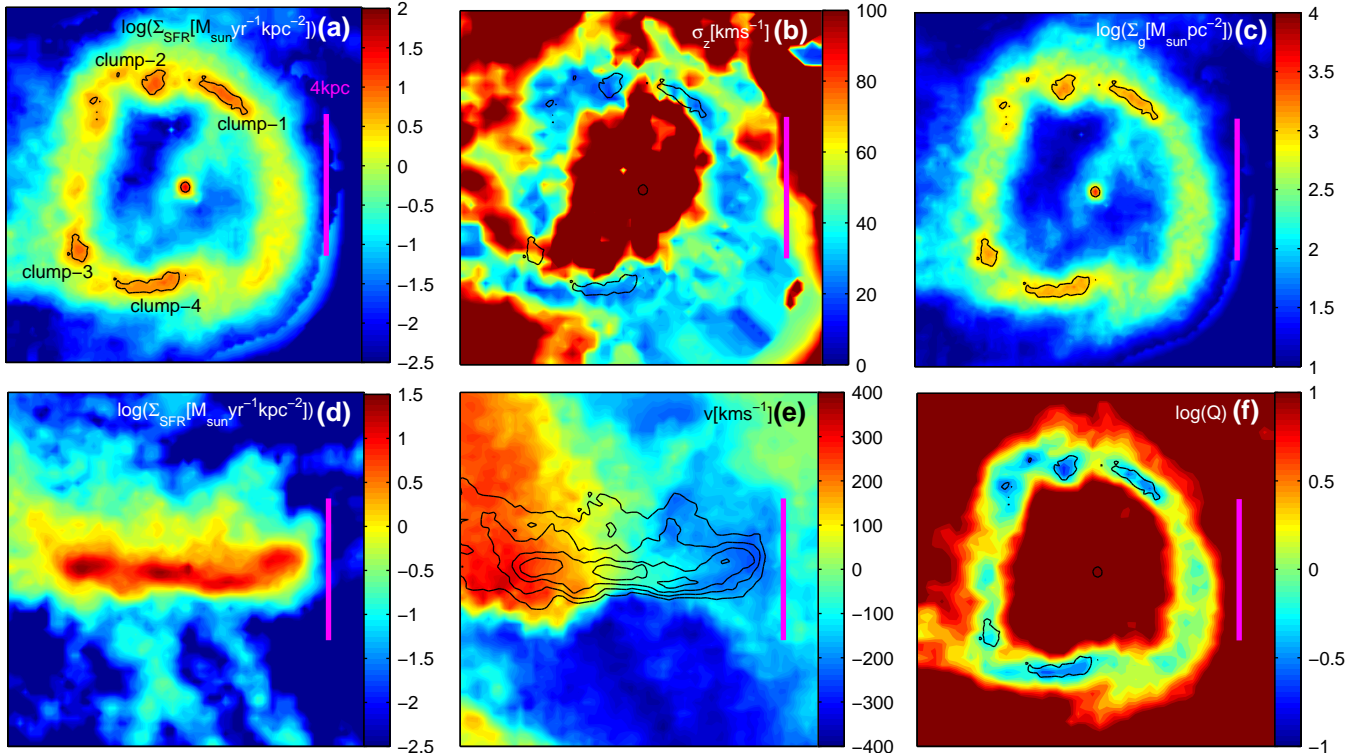


FIG. 2.— Gas properties of the central galaxy  $s224$  at  $z = 2$ . (a): face-on SFR surface density, (b): face-on line-of-sight (vertical) velocity dispersion, (c): face-on gas surface density, (d): edge-on SFR surface density, (e): edge-on line-of-sight velocity field overplotted with contours of SFR surface density and (f):  $\log Q$ . Each panel is 10 kpc on a side. All face-on panels are overplotted with  $\Sigma_g = 1000 M_\odot \text{pc}^{-2}$  contours.

following Herschel measurements (Nordon et al. 2010). Figure 1(b) shows ‘baryon conversion efficiencies’ ( $\frac{M_*}{M_{200\Omega_b/\Omega_m}}$ ) versus halo mass, where stellar masses are measured inside  $0.1R_{200}$ . Our simulated halos are presented (*symbols*) alongside the Moster et al. (2010) fit to observed mass functions (*black*). The baryon conversion efficiency is a strong function of mass in our simulations, though not as strong as observations suggest. Regardless, the global correlations in Figure 1 are a result of our wind model, without which they would compare much worse to the observations (Davé 2008, 2009). We consider these observed correlations important constraints that simulated galaxies should match in order to be realistic. A third global property of our simulations is high gas fractions,  $\sim 30\%$  for the central galaxies, in agreement with observations (Tacconi et al. 2010). The SFR history in the central galaxies is rather constant, as demonstrated in Table 1 by comparing the current SFR to its past average. Most central galaxies are clumpy (see below), as indicated in Table 1. Table 1 also gives halo masses, peak circular velocities, sizes, gas and stellar masses, gas fractions and SFRs.

We now discuss  $s224$ . The gas is mainly distributed in a ring at  $\approx 3$  kpc (Figure 2(c)). The ring, which is transient, formed from spiral features in the disk rather than by an interaction (there are no interactions with stellar mass ratios  $> 1 : 20$  since  $z \approx 3$ ). Several SFR overdensities are embedded in the ring (Figures 2(a) and 2(d)). Observationally, such regions are named giant clumps. Here for  $s224$  we use a threshold of face-on gas surface density  $\Sigma_g > 1000 M_\odot \text{pc}^{-2}$  to identify four clumps (Figure 2(a)). With this definition, their masses are  $\gtrsim 5 \times 10^8 M_\odot$  (Table 1). The gas vertical velocity dispersion  $\sigma_z$  is  $\approx 20 - 100 \text{ km s}^{-1}$  (Figure 2(b)), in agreement with observed values at  $z \approx 2$ . The high density

regions and clumps are minima of  $\sigma_z$  (Aumer et al. 2010), as denser gas dissipates the random motions more quickly and is less prone to stirring effects such as external accretion. The disk shows regular rotation (Figure 2(e)), indicative of the quiet merger history (Shapiro et al. 2008). The clumps themselves have low ( $\approx 50 \text{ km s}^{-1} \text{ kpc}^{-1}$ ) velocity gradients, not much larger than the galaxy-wide average velocity gradient, which is typically  $\approx 30 \text{ km s}^{-1} \text{ kpc}^{-1}$  at a few kiloparsecs from the center.

Assuming a  $Q$  parameter (Toomre 1964) of

$$Q \equiv \frac{\kappa \sqrt{\sigma_g^2 + c_s^2}}{\pi G \Sigma_g} \quad (3)$$

where  $\sigma_g$  is the local gas velocity dispersion,  $c_s$  the gas sound speed, and

$$\kappa = \sqrt{3} \sqrt{\frac{GM_{\text{tot}}(< R)}{R}} / R \quad (4)$$

(Dekel et al. 2009b), the clumps are local minima with  $Q \ll 1$  (Figure 2(f)). The clumps’ masses are 1–2 orders of magnitude larger than the thermal Jeans mass, but match the turbulent Jeans mass of the disk

$$M_{J,\sigma} \approx \left(\frac{\sigma_g}{v_{\text{rot}}}\right)^2 M_{\text{disk}} \gtrsim \left(\frac{20}{250}\right)^2 \times 6 \times 10^{10} M_\odot \approx 4 \times 10^8 M_\odot \quad (5)$$

(Genzel et al. 2008; Dekel et al. 2009b), which is driven to high values by the large random motions in the disk. The clumps tend to form inside spiral features, i.e. elongated overdensities in the disk, sometimes in transient rings, and reach a contrast ratio of  $\gtrsim 3$  compared to their surroundings or to

TABLE 1  
GALAXY AND CLUMP PROPERTIES

	$M_{200}$ [ $10^{12} M_{\odot}$ ]	peak $V_c \equiv \sqrt{\frac{GM}{R}}$ [ $\text{kms}^{-1}$ ]	Half-mass radius $R_{1/2}$ <sup>(a)</sup> [kpc]	Stellar mass <sup>(b)</sup> [ $10^{10} M_{\odot}$ ]	Gas mass <sup>(b)</sup> [ $10^{10} M_{\odot}$ ]	Gas fraction <sup>(b)</sup>	SFR <sup>(b)</sup> [ $M_{\odot} \text{ yr}^{-1}$ ]	Number of clumps <sup>(c)</sup>	$\frac{\text{SFR}}{\langle \text{SFR} \rangle}$ <sup>(d)</sup>
<i>s224</i>	1.48	278	3.3	3.82	2.04	35%	58.4	5	1.45
<i>s263</i>	1.75	289	3.3	3.43	2.06	37%	54	3	1.51
<i>s361</i>	1.02	238	4.6	2.12	0.78 <sup>(e)</sup>	27%	9.8 <sup>(e)</sup>	-	0.75 <sup>(e)</sup>
<i>s377</i>	1.38	252	4.5	2.75	1.19	30%	18.9	6	1
<i>s383</i>	1.38	253	3.5	2.96	0.96	25%	15	6	0.86
<i>s447</i>	0.95	229	3.8	1.74	1.29	43%	20.9	4	1.6
<i>clump-1</i>	-	-	0.45	0.022	0.044	67%	2.7	-	-
<i>clump-2</i>	-	-	0.27	0.02	0.04	67%	2.3	-	-
<i>clump-3</i>	-	-	0.22	0.022	0.025	53%	1.5	-	-
<i>clump-4</i>	-	-	0.42	0.027	0.07	72%	3.7	-	-

NOTE. — (a) For galaxies: stellar (3D) half-mass radius within  $0.2R_{vir}$ , for clumps: gas half-mass radius inside the region with  $\Sigma_g > 1000 M_{\odot} \text{ pc}^{-2}$ ; (b) For galaxies: inside  $2R_{1/2}$ , for clumps: inside the region with  $\Sigma_g > 1000 \text{ cm}^{-3}$ ; (c) Identified as local overdensities in the gas surface density, excluding the galaxy center; (d)  $\langle \text{SFR} \rangle$  is the mean SFR between  $z = 3$  and  $z = 2$ ; (e) The gas is mostly in an extended ( $> 2R_{1/2}$ ) massive ring, induced by a  $\approx 1 : 8$  merger, so the values here are underestimates.

the mean disk surface density. The total SFR in all clumps is  $\lesssim 20\%$  of the total disk SFR, in broad agreement with observations (Genzel et al. in prep.; Förster Schreiber et al. in prep.). The clumps are very gas rich ( $f_g \sim 60\%$ ), and are comprised of two stellar populations. ‘Background stars’, whose age distribution is similar to that of the stellar disk as a whole, are generally not bound to the clump. ‘Clump stars’, which form over the lifetime of the clump, are mostly bound to it, and constitute typically up to  $\approx 20\%$  of its *stellar* mass. Table 1 gives sizes, masses, gas fractions and SFRs for the clumps annotated in Figure 2(a).

A notable characteristic of the clumps is their short lifetimes, which are about half a disk orbital time, or  $\approx 50$  Myr. The top row in Figure 3 demonstrates the disruption of a clump in *s224* by showing a time series of gas surface density maps. In the upper right-most panel of Figure 3, the gas masses of three clumps are shown as a function of time (*solid*), demonstrating their rapid formation and disruption. In contrast, the bottom row of Figure 3 shows the evolution of the same clump in an experiment where we temporarily turn the wind off. The clump does not disrupt, instead it collapses further and virialises, and subsequently migrates to the galaxy center. This demonstrates that the clumps are destroyed by the wind feedback, and would survive (our equation-of-state is sufficiently soft to allow for this) similarly to previous simulations (Section 1) if this feedback was absent.

The reason for the disruption of clumps by the wind is the following. In our model, the wind mass-loading factor (i.e. the outflow rate over the SFR) for  $10^{10.5} M_{\odot}$  galaxies at  $z = 2$  is  $\eta \approx 3$  (Oppenheimer & Davé 2008), and the velocity ranges between  $\approx 350 - 750 \text{ kms}^{-1}$ . These wind parameters agree well with recent observational detections of gas outflowing from  $z \approx 2$  galaxies (Steidel et al. 2010) and clumps (Genzel et al. in prep.). Star-formation in the clumps proceeds on a timescale  $T_{SF} \approx 300$  Myr (according to the Kennicutt (1998) relation), thus winds drive gas out of the clumps on a timescale  $\approx T_{SF}/\eta \approx 100$  Myr, which is comparable to the disk orbital time. The consequence is that the gas surface density in the clumps decreases faster than the rate at which it is replenished by the instability inside the disk, and so clump regions move from  $Q \lesssim 1$  to  $Q \gtrsim 1$  (and thus stop collapsing) within a time that is shorter than the disk orbital time. The clumps typically convert just about 10% of their peak gas

mass into stars, hence the low fractions of ‘clump stars’ and high gas fractions inside the clumps. The short lifetimes we find are consistent with the *upper limits* of  $\approx 300 - 500$  Myr based on stellar population modelling (Elmegreen et al. 2009; Förster Schreiber et al. in prep.).

Given the masses and sizes of clumps (Table 1), their circular velocities equal  $\sqrt{GM/R} \approx 80 - 100 \text{ kms}^{-1}$ . This is significantly larger than the velocity dispersion of the gas within them or their rotational velocities (in particular if the galaxy-wide average velocity gradient is subtracted as ‘background’). Typically the clumps have  $v_{rot}^2 + 2\sigma_g^2 \approx 0.6(GM/R)$ , or  $|\frac{U}{K}| \gtrsim 3$ , where  $U$  is their gravitational potential energy and  $K$  the internal kinetic energy. Thus, they are neither supported by pressure nor by rotation, and in fact they are not virialised. This is due to continuous feedback on a timescale shorter than the dynamical time, that prevents virialisation before disruption.

#### 4. COMPARISON TO OBSERVATIONS

Figure 4 shows mock maps of  $H\alpha$  intensity, velocity and velocity dispersion, obtained by converting  $L_{H\alpha}[\text{ergs}^{-1}] = 1.26 \times 10^{41} \times \text{SFR}[M_{\odot} \text{ yr}^{-1}]$  (Kennicutt 1998), ‘placing’ *s224* at  $z = 2$ , convolving it with a FWHM =  $0.17''$  resolution, and pasting it into a real SINFONI datacube with pixel scale  $0.05''$ . This results in realistic resolution and noise properties that correspond to a representative total integration time ( $\approx 6$  hours) for our high-resolution SINFONI data sets (Förster Schreiber et al. 2009, Genzel et al. in prep.).

The clumpiness, smooth velocity field and relatively flat velocity dispersion map (outside the center), which are the characteristics of real SINS clumpy disks, are all well reproduced when ‘observing’ our simulations. The most significant difference to the non-degraded images in Figure 2 (the left and middle columns can be directly compared in Figures 4 and 2) is in the velocity dispersion map. The ‘beam smearing’ increases the apparent velocity dispersion where there are velocity gradients (this is the reason for the diagonal feature of high dispersion in the inclined image in Figure 4(c)), and the clumps are no longer seen as clear minima. As a result, the small but present velocity gradients across the clumps get smoothed out. Thus, because of the non-virialised state of the clumps, and their being minima in velocity dispersion, they do not show strong features in observations at the currently available resolution of  $\approx 1 - 2$  kpc, even if their masses are dynamically significant. This prediction is consistent with the

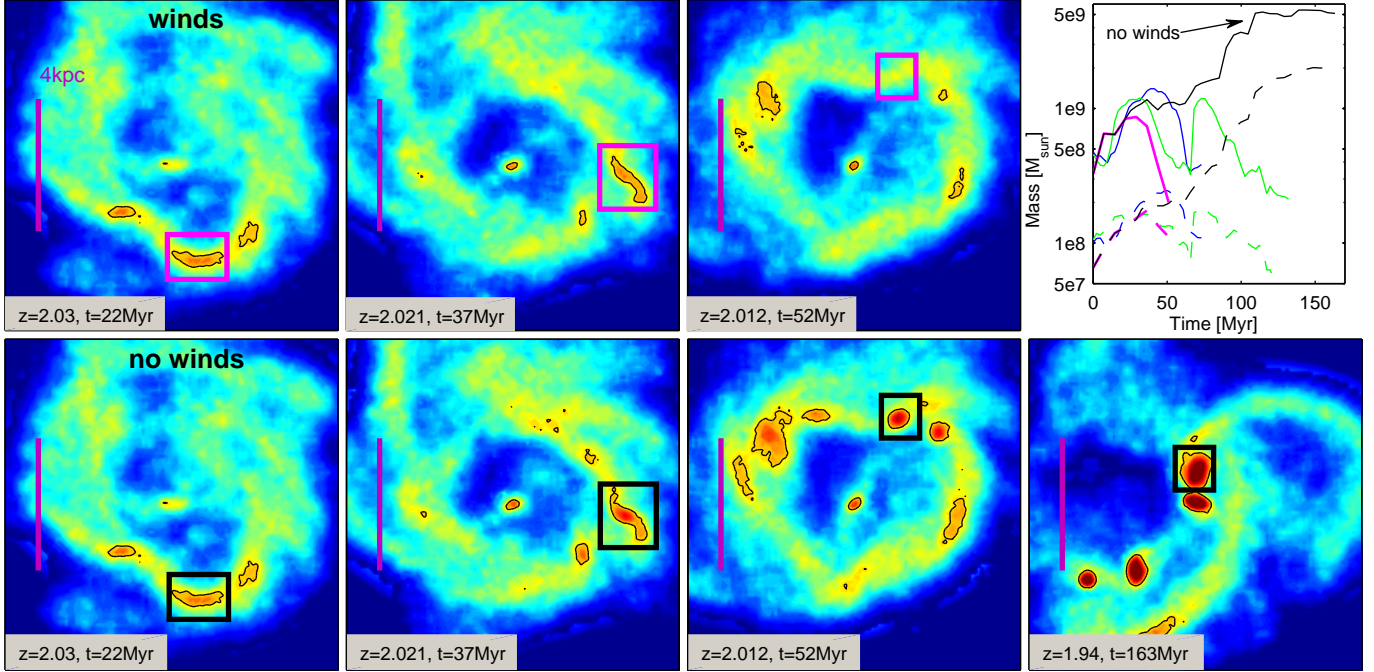


FIG. 3.— A time sequence of gas surface density maps showing the *disruption* of a clump in our model (*Top*), where  $t = 0$  (not shown) is the *formation* time of the clump. To demonstrate the role of the wind, we turn it off at  $z = 2.03$  and show the alternative evolution of non-disruption, virialisation and migration (*Bottom*). The color coding is as in Figure 2(c). The upper right-most panel shows the mass of gas (*solid*) and young ( $< 50$  Myr) stars (*dashed*) for four clumps as a function of time since their formation. The magenta lines are for the clump highlighted on the *Top* and the black for the clump highlighted on the *Bottom*. The jump in mass of the green lines at  $t \approx 60$  Myr is a result of a merger between two clumps (not shown in other panels). The typical clump lifetime in the presence of winds is  $\approx 50$  Myr, and the mass of new-formed stars is approximately 10% of the maximum clump gas mass. The mass of new-formed stars internal to the clump decreases following the decrease of the gas mass, as these stars are dispersed out of the clump when the collapse is halted by the return to  $Q > 1$ .

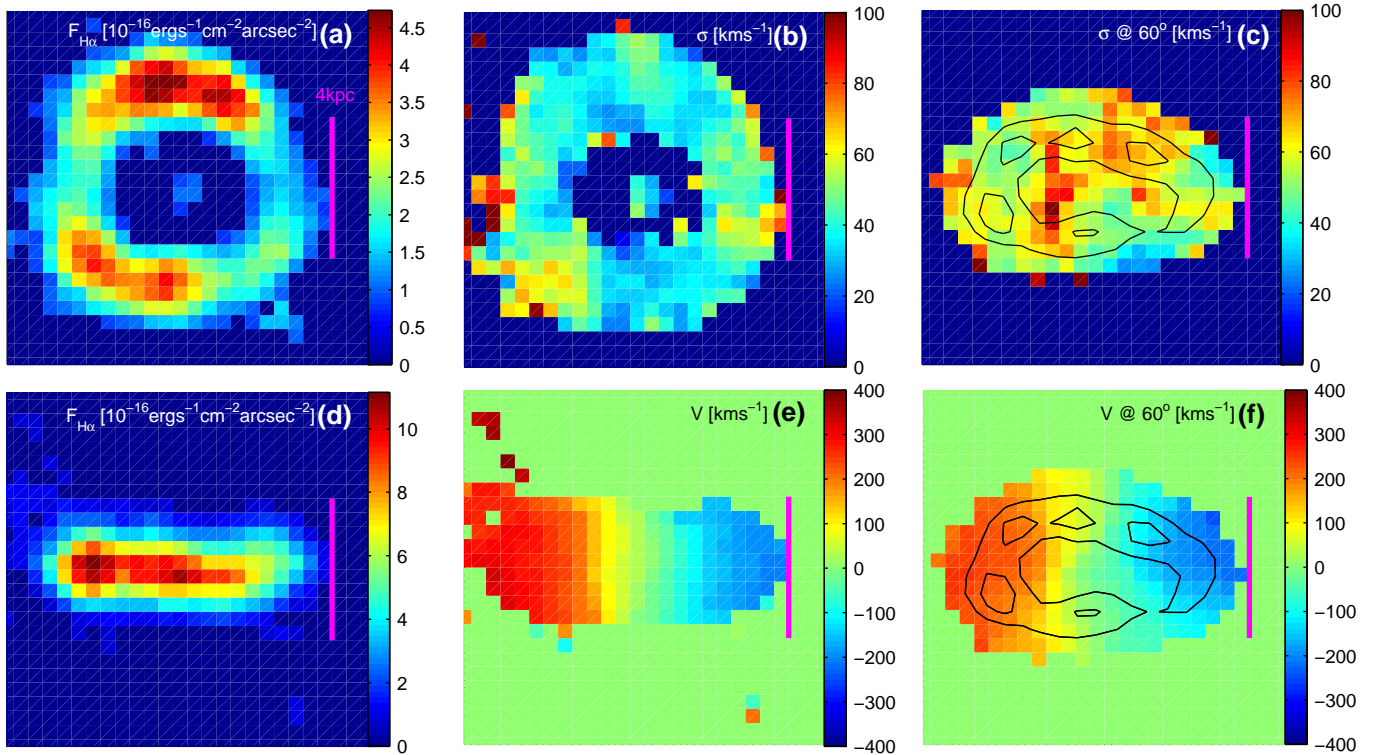


FIG. 4.— Mock  $H\alpha$  line observations of the snapshot shown in Figure 2, as would be obtained with SINFONI. Face-on (*a*) and edge-on (*d*) line intensity, velocity field shown edge-on (*e*) and at  $60^\circ$  inclination (*f*), and velocity dispersion shown face-on (*b*) and at  $60^\circ$  inclination (*c*). Contours of surface density are overlotted in panels (*c*) and (*f*). See Section 4 for discussion.

observations of Genel et al. (in prep.).

## 5. SUMMARY AND DISCUSSION

In this *Letter* we use 'zoom-in' cosmological hydrodynamical simulations that include a model for fast momentum-driven winds with high mass-loading factors to investigate the formation of star-forming disk galaxies at  $z \approx 2$ . Our wind model reproduces observed low baryon conversion efficiencies and high gas fractions, and we also find a good kinematical and morphological agreement with observations. In addition, we present an important numerical result, namely that the giant clumps in  $z \approx 2$  disks are short-lived and not virialised. This is because they are disrupted by feedback in less than a disk orbital time after they form and before they can reach virial equilibrium. We show that this scenario is plausibly consistent with the available observations.

Our results are in contrast to previous models that did not include fast winds with high mass-loading factors. Such winds are observed to be ubiquitous in high-redshift galaxies, and in particular they have been recently observed from individual giant clumps. We demonstrate that if we temporarily turn off the winds, we reproduce previous results where clumps are long-lived and migrate to the galaxy centers. However, if the wind is drastically reduced in a self-consistent way,

i.e. starting from the initial conditions at high redshift, a gas-rich unstable disk does not develop in the first place and the galaxies have very peaked rotation curves (e.g. Joung et al. 2009). An extensive exploration of parameter space will be described in Genel et al. (in prep.).

Our feedback recipe assumes that gas can be blown out of the clumps and subsequently out of the galaxy at high rates, as observed. It also assumes that star-formation always follows the Kennicutt (1998) relation, resulting in significant star-formation and wind expulsion even before the clump virialises. In the future it will have to be understood how this occurs on sub-clump scales based on improved physical models.

We thank Jerry Ostriker for useful discussions. The high performance computations were performed on the HLRB-II system provided by LRZ and on the SGI-Altix 3700 Bx2 (University Observatory Munich), partly funded by the Cluster of Excellence: "Origin and Structure of the Universe". We thank the DFG for support via German-Israeli Project Cooperation grant STE1869/1-1.GE625/15-1. SG acknowledges the PhD fellowship of the International Max Planck Research School in Astrophysics.

## REFERENCES

- Agertz, O., Teyssier, R., & Moore, B. 2009, *MNRAS*, L263+
- Aumer, M., Burkert, A., Johansson, P. H., & Genel, R. 2010, *ApJ*, 719, 1230
- Bournaud, F. et al. 2008, *A&A*, 486, 741
- Bournaud, F., Elmegreen, B. G., & Elmegreen, D. M. 2007, *ApJ*, 670, 237
- Burkert, A. et al. 2010, *ApJ*, in press (astro-ph/09074777)
- Ceverino, D., Dekel, A., & Bournaud, F. 2010, *MNRAS*, 404, 2151
- Cresci, G. et al. 2009, *ApJ*, 697, 115
- Daddi, E. et al. 2007, *ApJ*, 670, 156
- Davé, R. 2008, *MNRAS*, 385, 147
- Davé, R. 2009, in *Astronomical Society of the Pacific Conference Series*, Vol. 419, *Astronomical Society of the Pacific Conference Series*, ed. S. Jogee, I. Marinova, L. Hao, & G. A. Blanc, 347–+
- Dekel, A. et al. 2009a, *Nature*, 457, 451
- Dekel, A., Sari, R., & Ceverino, D. 2009b, *ApJ*, 703, 785
- Elmegreen, B. G., Bournaud, F., & Elmegreen, D. M. 2008, *ApJ*, 688, 67
- Elmegreen, B. G., Elmegreen, D. M., Fernandez, M. X., & Lemonias, J. J. 2009, *ApJ*, 692, 12
- Elmegreen, B. G., Elmegreen, D. M., Vollbach, D. R., Foster, E. R., & Ferguson, T. E. 2005, *ApJ*, 634, 101
- Finlator, K., & Davé, R. 2008, *MNRAS*, 385, 2181
- Förster Schreiber, N. M. et al. 2009, *ApJ*, 706, 1364
- . 2006, *ApJ*, 645, 1062
- Genel, S. et al. 2008, *ApJ*, 688, 789
- Genzel, R. et al. 2008, *ApJ*, 687, 59
- . 2006, *Nature*, 442, 786
- Gnedin, N. Y., Tassis, K., & Kravtsov, A. V. 2009, *ApJ*, 697, 55
- Haardt, F., & Madau, P. 2001, in *Clusters of Galaxies and the High Redshift Universe Observed in X-rays*, ed. D. M. Neumann & J. T. V. Tran
- Immeli, A., Samland, M., Westera, P., & Gerhard, O. 2004, *ApJ*, 611, 20
- Joung, M. R., Cen, R., & Bryan, G. L. 2009, *ApJ*, 692, L1
- Kennicutt, R. C. 1998, *ARA&A*, 36, 189
- Kereš, D., Katz, N., Weinberg, D. H., & Davé, R. 2005, *MNRAS*, 363, 2
- Krumholz, M. R., & Dekel, A. 2010, *MNRAS*, 406, 112
- Martin, C. L. 2005, *ApJ*, 621, 227
- Moster, B. P., Somerville, R. S., Maulbetsch, C., van den Bosch, F. C., Macciò, A. V., Naab, T., & Oser, L. 2010, *ApJ*, 710, 903
- Murray, N., Quataert, E., & Thompson, T. A. 2005, *ApJ*, 618, 569
- . 2010, *ApJ*, 709, 191
- Nordon, R. et al. 2010, *A&A*, 518, L24+
- Oppenheimer, B. D., & Davé, R. 2006, *MNRAS*, 373, 1265
- . 2008, *MNRAS*, 387, 577
- Oser, L., Ostriker, J. P., Naab, T., Johansson, P. H., & Burkert, A. 2010, *ApJ*, submitted (astro-ph/10101381)
- Pettini, M., Steidel, C. C., Adelberger, K. L., Dickinson, M., & Giavalisco, M. 2000, *ApJ*, 528, 96
- Rupke, D. S., Veilleux, S., & Sanders, D. B. 2005, *ApJS*, 160, 115
- Sales, L. V., Navarro, J. F., Schaye, J., Vecchia, C. D., Springel, V., & Booth, C. M. 2010, *MNRAS*, 1326
- Schaye, J., & Dalla Vecchia, C. 2008, *MNRAS*, 383, 1210
- Shapiro, K. L., Genel, R., & Förster Schreiber, N. M. 2010, *MNRAS*, 403, L36
- Shapiro, K. L. et al. 2008, *ApJ*, 682, 231
- Springel, V. 2005, *MNRAS*, 364, 1105
- Springel, V., & Hernquist, L. 2003, *MNRAS*, 339, 289
- Steidel, C. C., Erb, D. K., Shapley, A. E., Pettini, M., Reddy, N., Bogosavljević, M., Rudie, G. C., & Rakic, O. 2010, *ApJ*, 717, 289
- Tacconi, L. J. et al. 2010, *Nature*, 463, 781
- Toomre, A. 1964, *ApJ*, 139, 1217
- Zhang, D., & Thompson, T. A. 2010, *ApJ*, submitted (astro-ph/10054691)